Dislocation nucleation and defect structure during surface indentation

Cynthia L. Kelchner

Sandia National Laboratories, Livermore, California 94551-0969

S. J. Plimpton

Sandia National Laboratories, Albuquerque, New Mexico 87185

J. C. Hamilton

Sandia National Laboratories, Livermore, California 94551-0969

We model indentation of a metal surface by combining an atomistic metal with a hard-sphere indenter. This work provides atomistic imaging of dislocation nucleation during displacement controlled indentation on a passivated surface. Dislocations and defects are located and imaged by local deviations from centrosymmetry. For a Au(111) surface, nucleation of partial dislocation loops occurs below the surface inside the indenter contact area. We compare and contrast these observations with empirical criteria for dislocation nucleation and corresponding continuum elasticity solutions. [S0163-1829(98)02141-9]

Mechanical deformation, fracture, and friction of solids and thin films pose some of the most interesting computational challenges for atomistic calculations of materials properties. The fundamental goal is to establish a connection between atomic scale processes and measurable mechanical properties of materials. The development of nanoindentation techniques,[1] atomic-force microscopy,[2] and the interfacial force microscope[3,4] (IFM) has generated considerable interest in the detailed mechanisms of deformation during indentation at a very small scale. Indentation techniques measure the mechanical properties of thin films and other materials (e.g., elastic constants, yield stress, and hardness) by measuring the force or load on the indenter tip as a function of the tip displacement during indentation and retraction.

The classical problem of an isotropic elastic material filling a half space and indented by a spherical frictionless indenter was solved by Hertz[5] and has been extended to anisotropic media and to a variety of indenter shapes.[6] However, real indentation experiments also involve plastic deformation, i.e., plastic flow and the creation of defects, which can be studied with atomistic calculations. In this paper, we present a computational model that couples a frictionless indenter, represented here by a repulsive potential, with atomistic calculations to study the elastic and plastic deformation during indentation on a passivated surface. Combined with an approach for imaging defects, this provides insight into the initial stages of plastic deformation which had previously been unavailable.

Previous atomistic calculations have studied indentation and retraction using the embedded-atom method (EAM),[7,8] or other semiempirical techniques,[9] as well as first-principles methods.[10] These calculations showed strong bonding between the indenter tip and the surface due to the large energy of adhesion between two clean surfaces. This leads to a jump to contact upon approach and necking between the tip and surface during retraction.[7,11]

In experiments, the tip-surface adhesive interaction will be dramatically reduced if the tip and surface are not atomi-

cally clean. Surfaces in ambient atmospheres, for example, often have passivating layers of oxide.[12] In other experiments, surfaces are passivated by the addition of an alkanethiol layer which prevents bonding between the tip and the surface.[4,13] The model discussed here is tailored to address these thiol passivated surfaces, as well as to reproduce the salient features of displacement controlled indentation experiments.[3,4] Interpretation of experimental force vs displacement curves requires understanding the atomistic structures of dislocations and other defects created during indentation. Such an understanding will help resolve disagreement in the literature regarding yield stresses and mechanisms leading to plastic flow under indentation.

We model the effect of a passivation layer by using a strong repulsive potential to represent the indenter tip. Each atom in the indented material interacts with the idealized indenter via the potential $V(r) = A\theta(R-r)(R-r)^3$, where A is a force constant, $\theta(R-r)$ is the standard step function, R is the indenter radius, and r is the distance from the atom to the center of the indenter sphere. We chose this particular potential in order to avoid the numerical problems during energy minimization caused by a perfectly hard-sphere potential. There is no force in the direction tangent to the tip sphere. The model is therefore analogous to the Hertzian indenter in that it is frictionless, similar to the lubricant effect of the thiol passivating layer.[13]

Minimum energy calculations were performed for indentation on a Au(111) surface, using a repulsive potential with $A = 5.3$ nN/Å^2 to model a spherical indenter with an 80 Å radius. (Related experiments[14] used indenter tips with radii as small as 250 Å, but atomistic calculations for these are still prohibitive.) The gold surface was represented by a slab of dimension $240 \times 210 \times 160$ Å containing 470 000 atoms. Periodic boundary conditions were used parallel to the surface, and the bottom layer was held fixed. To ensure that these boundary conditions did not affect the results, calculations were also run on smaller rectangular slabs and on a threefold symmetric triangular slab with fixed boundaries on
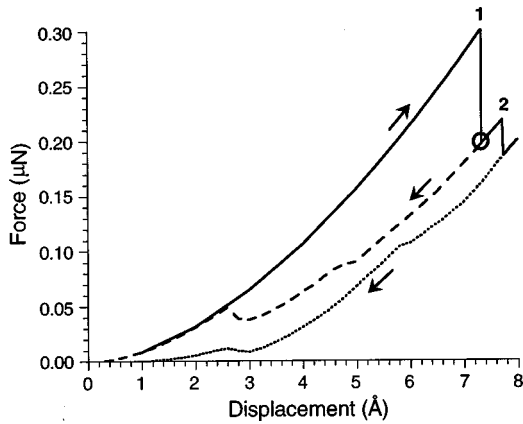
FIG. 1. Force vs displacement curve for Au(111) during indentation (solid line) of a spherical tip with 80 Å radius and during retraction (dashed lines) after the first (**1**) and second (**2**) plastic yield points. The circle marks the point where the structure in Fig. 2 was obtained.

the sides and bottom layer. Results for such cases are essentially identical. The indenter displacement d was changed in small steps (0.1 to 1 Å) and at each step the total energy was minimized at 0 K, using a conjugate gradient algorithm and an EAM potential for Au.[15] In the vicinity of plastic yield points, smaller steps (0.01 Å) were used to verify that the resulting dislocation structure did not depend on the step size. We chose this approach to mimic the quasiequilibrium IFM experiments.[3,4] We also studied dislocation nucleation using short molecular-dynamics (MD) runs, as described later in this paper. All calculations were run with the PARADYN code.[16]

The force vs displacement curves for indentation and retraction are shown in Fig. 1. Initially, the indentation curve follows the Hertzian solution for elastic deformation where $F = Kd^{3/2}$.[5] The indentation modulus derived from the fitting constant K is 118 GPa, whereas the experimental value is 85 GPa measured with a tip radius of 700 Å.[17] The force F on the indenter decreases abruptly when the elastic stress under the indenter is partially relieved by plastic deformation in the thin film, in excellent agreement with experimental results.[17] When the indenter tip is retracted after reaching the first yield point in Fig. 1, the force at small displacements matches that during indentation. This indicates that the plastic deformation created at the first yield point has healed during retraction. In contrast, the force profile during retraction from the second yield point indicates permanent deformation after retraction.

In order to study the structures of the plastically deformed thin film in detail, the location and type of defects present must be reliably identified. Separating the defects from the extensive elastic deformation in the thin film is not a trivial problem. Techniques relying on the electron density, the potential energy, the dislocation density tensor,[18] or the atomic level stress tensor[19] for each atom often identify regions of elastically deformed material in addition to the defected material. Instead, we have exploited the fact that a centrosymmetric material (such as gold or other fcc metal) will remain centrosymmetric under homogeneous elastic deformation. In a centrosymmetric material, each atom has pairs of equal and opposite bonds to its nearest neighbors. As the material is

distorted, these bonds will change direction and/or length, but they will remain equal and opposite. When a defect is introduced nearby, this equal and opposite relation no longer holds for all of the nearest-neighbor pairs. Thus we can define a centrosymmetry parameter which is zero for a centrosymmetric material under any homogeneous elastic deformation but nonzero for any plastic (i.e., nonelastic) deformation of the material.

The centrosymmetry parameter for each atom is defined as follows:

$$P = \sum_{i=1,6} |\mathbf{R_i} + \mathbf{R_{i+6}}|^2,$$

where $\mathbf{R_i}$ and $\mathbf{R_{i+6}}$ are the vectors or bonds corresponding to the six pairs of opposite nearest neighbors in the fcc lattice. The 12 nearest-neighbor vectors for each atom are first determined in an undistorted bulk fcc lattice with the orientation of the slab. The analogous set of 12 vectors for each atom in the distorted lattice $\mathbf{R_i}$ is then generated by finding those neighbors in the distorted lattice with vectors closest in distance to the undistorted nearest-neighbor vectors. It is possible that this set will contain duplicates or nonnearest neighbors if a given atom has fewer than 12 nearest neighbors or a very distorted local environment. Each ''equal and opposite'' pair of vectors is added together, then the sum of the squares of the six resulting vectors is calculated. This final number is a measure of the departure from centrosymmetry in the immediate vicinity of any given atom and is used to determine if the atom is near a defect.

For reference, the centrosymmetry parameter is zero for atoms in a perfect Au lattice, 24.9 Å^2 for surface atoms, 8.3 Å^2 for atoms in an intrinsic stacking fault, and 2.1 Å^2 for atoms halfway between fcc and hcp sites (i.e., in a partial dislocation). These values assume that the gold nearest-neighbor distance does not change in the vicinity of these defects. We find in practice that the centrosymmetry parameter can readily distinguish between these three types of environments.

Figure 2 shows three views of the dramatic defect structure after the first plastic deformation event (at the circle in Fig. 1). The atoms are colored according to the value of the centrosymmetry parameter with red for partial dislocations ($P = 0.5–4.0$), yellow for stacking faults ($P = 4.0–20$), and white for surface atoms ($P > 20$). These ranges were chosen based on the values for the different environments given in the previous paragraph. Note that Fig. 2 does not allow identification of the Burgers vectors. The stacking faults are bounded by the partial dislocation loops, which start at the surface and reach a depth of 85 Å into the thin film. All of the defects in this system lie on {111} planes which are the energetically preferred slip planes in the fcc lattice. From the (111) surface, there are three unique {111} planes extending into the bulk. In this structure, defects can be seen parallel to only two of these three planes.

The structure shown in Fig. 2 is complex and it is beyond the scope of this paper to catalog the many dislocation lines and Burgers vectors involved. A simpler but fundamental question regards the nucleation of this defect structure. By using MD and the centrosymmetry parameter, we were able to image the nucleation of the partial dislocation loops. The
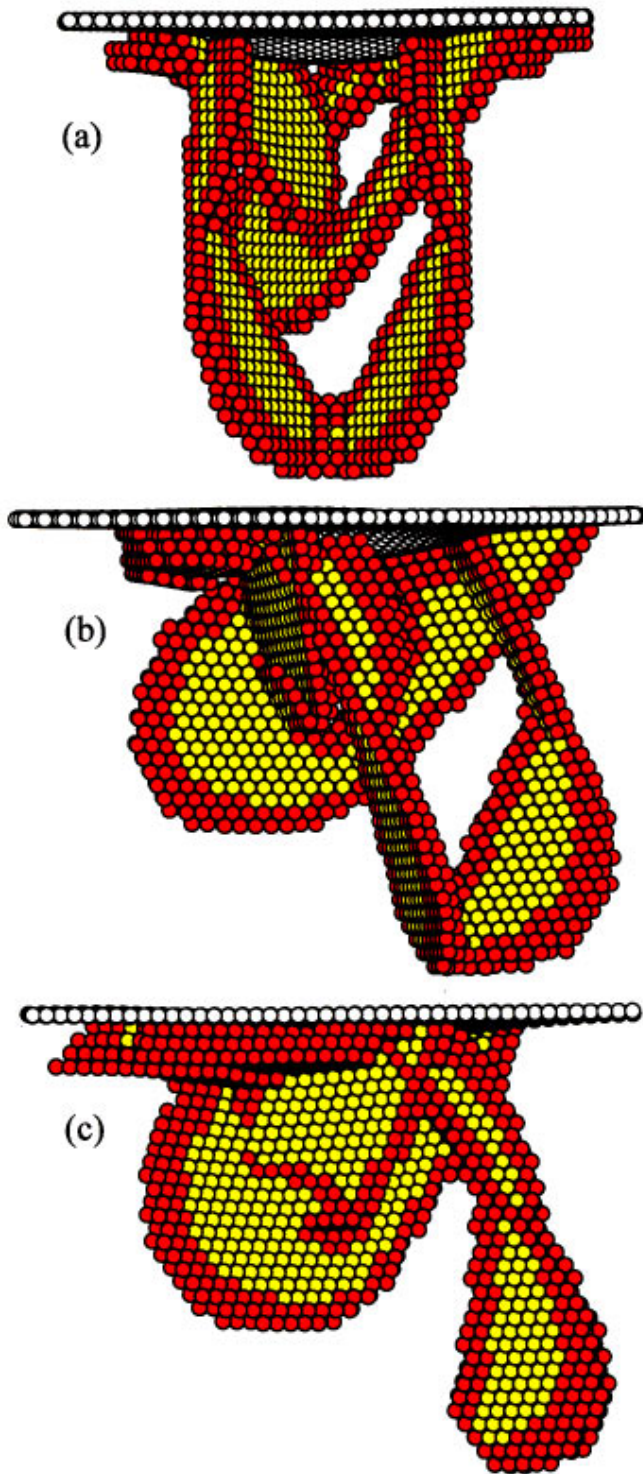
FIG. 2. (Color). Defect structure at the first plastic yield point during indentation on Au(111), (a) view along $[11\bar{2}]$, (b) rotated 45° about $[111]$, and (c) rotated 90° to $[1\bar{1}0]$. The colors indicate defect types as determined by the centrosymmetry parameter: partial dislocation (red), stacking fault (yellow), and surface atoms (white). Only atoms with $P > 0.5$ are shown.
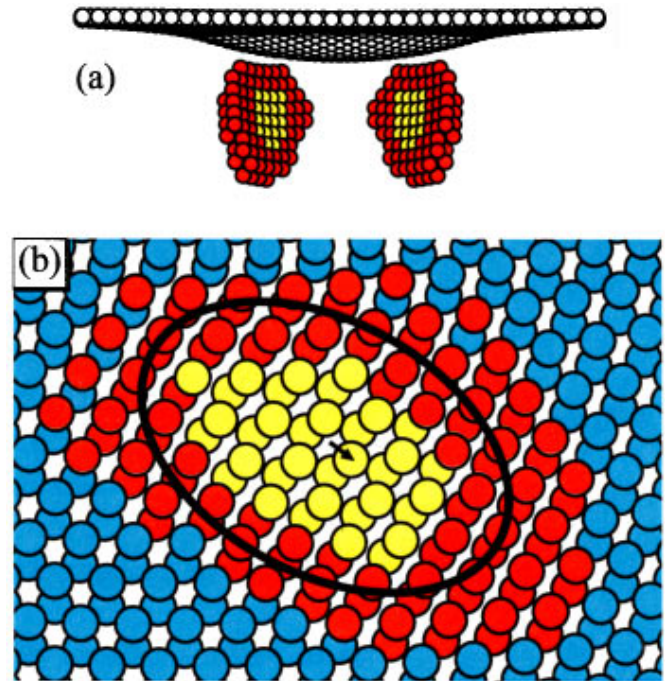

FIG. 3. (Color). Snapshot during dislocation nucleation at the first plastic yield point on Au(111), (a) same view and colors as Fig. 2(a), (b) a two-layer-thick cross section of a $(\bar{1}11)$ plane containing the partial dislocation loop on the right in (a), where all atoms are now shown ($P < 0.5$ in blue) and the partial dislocation line and stacking fault Burgers vector are marked. The partial Burgers vector lies along $\langle \bar{1}21 \rangle$.

starting geometry for the MD run was that at label **1** in Fig. 1, and the tip displacement was held to that at the circled point in Fig. 1. We found that partial dislocation loops first appear with mirror symmetry at approximately half of the contact radius beneath the surface. Figure 3 presents two different views of these initial partial dislocation loops. The dislocation lines and Burgers vectors of the nucleating dislocation loops were obtained by examining appropriate Burgers circuits on the {111} planes containing the partial dislocations. These dislocation loops grow rapidly into the solid, emerge at the surface, and interact to produce the structure shown in Fig. 2. The MD run was continued long enough for the loops to equilibrate via a complex series of dislocation reactions (on the order of picoseconds).

The nucleation of dislocation loops off the indenter axis was not expected when we began these calculations. A commonly used empirical criterion for dislocation nucleation is that the maximum-resolved shear stress (MRSS) exceed the critical shear stress for the indented material.[20] From continuum elasticity theory,[21] the MRSS is on the indenter axis and on a plane at 45° from the axis. Hence it has generally been assumed that dislocations nucleate on the indenter axis. However, our simulation results show unequivocally that this is not the case for the (111) surface of single crystal Au. This occurs because the {111} slip planes are at an angle of 71° from the (111) surface plane. Reexamination[22] of the elasticity solution for the shear stress off-axis[23] shows that the largest shear stress resolved on the {111} planes occurs off-axis, in agreement with our predictions. This significant consequence of the continuum elasticity solution had not been appreciated previously.

The largest shear stress resolved on the {111} planes calculated just before the first yield point in our simulations was 7 GPa. Using the same EAM potential, the calculated critical shear stress for bulk Au is 2 GPa. Clearly the usual empirical

criterion for the plastic yield mentioned above is not a good approximation at these very small length scales. A more rigorous criterion for nucleation of plastic deformation is that the work done over the displaced surface be greater than the line energy of the new dislocation loop. As the indenter size decreases to the nearly atomistic scale, the volume having a maximum shear stress decreases until it is comparable to the dislocation linewidth. At this small length scale, the average shear stress over the nucleating dislocation loop will be less than the maximum shear stress. This, combined with surface effects on the line energy and image forces near the surface, results in a maximum resolved shear stress at yield (7 GPa) larger than the calculated critical shear stress of Au (2 GPa).

The loss of the (111) surface's threefold symmetry upon indentation appears to be a fundamental property of the glide process along two of the three {111} planes. The orientation of the dislocation structure can vary with the initial conditions of the simulation such as the indenter aiming point and the symmetry (twofold or threefold) of the boundary conditions, but we never obtain a threefold symmetric defect structure.

In summary, this work provides atomistic imaging of dislocation nucleation in a passivated surface under displacement controlled indentation. Our computational model probes both the elastic deformation regime of the Hertzian indenter and the plastic deformation regime of mechanical testing on passivated surfaces. The method we have developed to identify the defects clearly distinguishes between elastic and plastic deformation. In another paper we will discuss similar calculations for the Au (001) and (110) surfaces.[24] Each surface produces unique dislocation structures, and force vs displacement curves, due to the orientation of the {111} slip planes relative to the surface. These detailed structures provide a basis for understanding plastic deformation during the indentation and retraction processes and therefore the mechanical properties of the thin film.

[1] J. S. Field and M. V. Swain, J. Mater. Res. **10**, 101 (1995); W. C. Oliver and G. M. Pharr, *ibid.* **7**, 1564 (1992).

[2] W. W. Gerberich *et al.*, Acta Mater. **44**, 3585 (1996); E. Lilleodden *et al.*, J. Mater. Res. **10**, 2162 (1995).

[3] S. A. Joyce and J. E. Houston, Rev. Sci. Instrum. **62**, 710 (1991).

[4] P. Tangyunyong *et al.*, Phys. Rev. Lett. **71**, 3319 (1993).

[5] H. Hertz, J. Reine Angewandte Math. **92**, 156 (1882).

[6] J. J. Vlassak and W. D. Nix, J. Mech. Phys. Solids **42**, 1223 (1994).

[7] U. Landman and W. D. Luedtke, J. Vac. Sci. Technol. B **9**, 414 (1991); U. Landman, W. D. Luedtke, N. A. Burnham, and R. J. Colton, Science **248**, 454 (1990).

[8] J. Belak, D. B. Boercker, and I. F. Stowers, MRS Bull. **18**, 55 (1993).

[9] D. W. Brenner *et al.*, Nanotechnology **7**, 161 (1996); J. S. Kallman *et al.*, Phys. Rev. B **47**, 7705 (1993).

[10] R. Pérez, M. C. Payne, and A. D. Simpson, Phys. Rev. Lett. **75**, 4748 (1995).

[11] L. Kuipers and J. W. M. Frenken, Phys. Rev. Lett. **70**, 3907 (1993).

[12] S. K. Venkataraman, D. L. Kohlstedt, and W. W. Gerberich, J. Mater. Res. **8**, 685 (1993).

[13] R. C. Thomas *et al.*, Science **259**, 1883 (1993); S. A. Joyce *et al.*, Phys. Rev. Lett. **68**, 2790 (1992).

[14] T. A. Michalske and J. E. Houston, Acta Mater. **46**, 391 (1998).

[15] S. M. Foiles, M. I. Baskes, and M. S. Daw, Phys. Rev. B **33**, 7983 (1986).

[16] S. J. Plimpton and B. A. Hendrickson, in *Materials Theory and Modelling*, edited by J. Broughton, P. Bristowe, and J. Newsam, MRS Proceedings No. 291 (Materials Research Society, Pittsburgh, 1993).

[17] J. D. Kiely and J. E. Houston, Phys. Rev. B **57**, 12 588 (1998).

[18] M. S. Daw *et al.*, in *Modeling Environmental Effects on Crack Growth Processes*, edited by R. H. Jones and W. W. Gerberich (Metallurgical Society, Warrendale, PA, 1986); E. Kröner, in *Physics of Defects*, edited by R. Balian, M. Kléman, and J.-P. Poirier (North-Holland, Amsterdam, 1981).

[19] D. T. Kulp, G. J. Ackland, M. Sob, V. Vitek, and T. Egami, Modell. Simul. Mater. Sci. Eng. **1**, 315 (1993).

[20] J. P. Hirth and J. Lothe, *Theory of Dislocations* (Krieger, Malabar, FL, 1982), p. 6.

[21] K. L. Johnson, *Contact Mechanics* (Cambridge University Press, Cambridge, 1985), p. 95; R. M. Davies, Proc. R. Soc. London, Ser. A **197**, 416 (1949).

[22] J. D. Kiely and J. E. Houston (private communication).

[23] G. M. Hamilton, Proc. Inst. Mech. Eng. Part C **197**, 53 (1983).

[24] C. L. Kelchner and J. C. Hamilton (unpublished).